Stress transmission in porous materials impacted by shock waves

Vahid Kazemi-Kamyab, Kolluru Subramaniam, and Yiannis Andreopoulos

Citation: Journal of Applied Physics **109**, 013523 (2011); doi: 10.1063/1.3517791
View online: http://dx.doi.org/10.1063/1.3517791
View Table of Contents: http://scitation.aip.org/content/aip/journal/jap/109/1?ver=pdfcov
Published by the AIP Publishing

Stress transmission in porous materials impacted by shock waves

Vahid Kazemi-Kamyab,[1,a)] Kolluru Subramaniam,[2] and Yiannis Andreopoulos[1,b)]
[1]*Department of Mechanical Engineering, The City College of the City University New York, Convent Avenue, 140th Street New York, New York 10031, USA*
[2]*Department of Civil Engineering, The City College of the City University New York, Convent Avenue, 140th Street New York, New York 10031, USA*

(Received 26 March 2010; accepted 25 October 2010; published online 13 January 2011)

The interaction of moving shock waves with short length elastic porous aluminum samples of various porosities was investigated in a shock tube facility in a setup where the specimens were placed in front of a long rod of a modified Hopkinson Bar. High frequency response miniature pressure transducers and semiconductor strain gages were used to measure the pore gas pressure and the transmitted stress wave to the rod respectively. It was found that the effect of pore gas flow on the total stress history was inversely proportional to the material's porosity, permeability and length. For low porosity aluminum samples due to the very low and very confined volumetric gas flow rate within the foam, a minimal contribution of the gas pressure within the pores to the total stress was observed and the magnitude of stress wave transmitted to the rod was amplified mainly due to the lower acoustic impedance of the foams relative to the rod. However, in a high porosity aluminum specimens with a high permeability and low inertial coefficient, there is a high volumetric gas flow rate within the foam, where faster wave interactions within the gas phase take place resulting in an earlier arrival of the rarefaction wave and restricting the magnitude of the total stress to reach its value when no gas flow into the pores is allowed. Due to this out of phase interaction between the wave propagating within the gas phase and the fast wave propagating in the solid matrix, the magnitude of the stress wave transmitted to the rod was slightly attenuated when the high porous foam was placed in front of the rod. It was also found that the aluminum foams deviate from a linearly elastic medium behavior and demonstrate dispersive and dissipative properties which result in the gradual rise or fall of the stress and damping of the oscillations. The pore gas flow influences the profile of the oscillations by introducing dissipation and dispersion into the propagating wave in the solid phase due to the nonlinear nature of the solid-fluid interaction. Further data analysis included a decomposition of the measured time-dependent signals into two components, one with low frequency content which is argued that it is associated with Biot's slow wave and one with high frequency contributions which corresponds to the fast wave propagation. It is also argued that this decomposition can differentiate the effects of gas pressure in the pores from the stress in the matrix of the porous medium. © *2011 American Institute of Physics*. [doi:10.1063/1.3517791]

I. INTRODUCTION

Research on the propagation of nonlinear waves in porous media is among the fundamental research topics in mechanics. Of particular interest is the interaction of shock waves with gas-solid mixtures. It is reasonably well documented that shock waves propagating in foams or porous materials are attenuated,[1,2] and such accurately controllable shock attenuations are widely used in various engineering and industrial applications such as the design of safety shells for protection and mitigation from explosions, porous structures for noise reduction in high speed railway tunnels, and underwater shock wave interaction with soft organs in human body (lithotripsy). Early studies of the interaction of shock waves with porous media were done within the context of finding materials to attenuate and dissipate the energy associated with shock and blast wave loading.[3] In shock wave applications to medicine, for example, the focused underwater shock waves interaction with human tissues is considered to cause tissue damage which is attributed to pressure amplification. There are also studies related to the thermodynamic processes in interactions between shock wave, bubbly liquid, dusty, or mist flow.[4,5] Research on the propagation of nonlinear waves in porous media may also lead to developing methodologies for the identification of different underground fluid pockets and for cleaning groundwater from trapped contaminants, which are localized at specific sites.

Classical attempts to model these phenomena start from the microscopic conservation laws (mass, momentum, and energy) from which macroscopic evolution equations (ordinary and partial differential equations) are derived, complemented by appropriate closures. The single phase approach of Mazor *et al.*[6] was one of the first developed to describe shock interactions with cellular materials, but with limited results. A more sophisticated approach in which various phases interact with each other is available,[7] but suffers from a crude treatment of the solid medium. The first study which seriously includes fundamental porous media mechanics is that of Biot[8] on compression wave propagation. A large num-

[a)]Present address: Faculty of Aerospace Engineering, Delft University of Technology, P. O. Box 5058, 2600 GB Delft, The Netherlands.
[b)]Electronic mail: andre@ccny.cuny.edu.

ber of papers have appeared in the literature following Biot's pioneering work, referring to microscopic representations of the phase balance equations within the framework of the theory of mixtures, but applying these concepts to nonlinear waves led to poor results. A more accurate representation of the momentum and energy processes at the internal surfaces of the porous medium was introduced in Levy *et al.*[9] by including the Forchheimer term in the model of Bear and Bachmat.[10] The basic paradox of these equations is that although they are inviscid in nature, so that the shock wave motion is adequately captured and resolved, the Forchheimer term, which approximately accounts for energy losses inside the pores, contains viscous effects.

Generally, the detailed mechanisms of shock wave attenuation in interactions with complex solids such as porous media, cellular materials, packed granular materials, or biological tissues are not yet understood because of the extremely complex phenomena involved. Even though the interaction of shock wave with porous materials is highly nonlinear,[11] linear wave theory can be applied in order to get insight into the behavior of the pore fluid and the skeleton of the porous material and their interaction as the material is impacted by the shock wave. The process of interaction of a shock wave with the surface of a porous material involves a partial reflection of the shock in the opposite direction, a partial refraction/transmission of the shock into the porous material and the generation of stress waves. It can be mathematically derived that upon the shock wave loading of the saturated porous material, the initial step-wise perturbation is split into two parts (for detailed derivation consult[12,13]): the first wave in which pore fluid and porous material are compressed simultaneously, i.e., the solid and fluid particles have in phase motion, and a second wave in which the pore fluid is compressed again, while the porous material relaxes, i.e., the two phases have an out of phase motion. In some papers these two waves are known as deformation (fast, mode 1) and filtration (slow, mode 2) waves. The relative energy distribution of the two waves depends on the boundary conditions including pore characteristics, fluid-solid phase density ratio and compressibility contrast. For stiff porous material structures the compressibility contrast is large, the two waves are effectively decoupled, the amplitude of the first mode in the fluid pressure is too low to be detected in the fluid pressure measurements and the amplitude of the second mode cannot be detected in the solid matrix.

One of the earliest experimental attempts to investigate shock wave interaction with rigid porous materials was carried out by Grinten.[12] The porous material, 2 m in length, consisted of sand particles fixed together by epoxy. It was found that the pressure inside the sample increases gradually and no wave structure is evident in the pressure signals, suggesting that the wave propagation through the material is fully dispersed. In addition, the fluid-solid interaction has a nonlinear nature as a nonlinear drag law known as Forchheimer term in the momentum transport equation, was shown to best fit the data.

In similar experiments, Levy *et al.*[14] investigate the impact of shock waves on open cell silicon carbide (SiC) and alumina (Al_2O_3) with pore sizes and porosities ranging from 20–40 ppi and $\Phi = 72\% - 82\%$ (of air), respectively. This work showed that the transmitted compaction wave in the fluid phase has a sharp front followed by a continuous pressure increase. The sharp front decays as the compaction wave travels further into the material. There is no clear evidence of the reflection of the compaction wave off the end wall of the tube. This observation is further supported by the fact that the end wall pressure did not remain uniform. The final pressure is higher than the pressure that would have been obtained if the wave was reflected off a rigid wall. From the above observations, it can be inferred that the compaction wave broadens as it travels through the specimen and becomes dispersed. The transmitted wave interacts with the pore structure at the front edge of the porous material, to generate multiple reflections, diffractions, and interactions which are fed back into the external flow and eventually join to form the reflection wave.

In general, waves through porous materials will be attenuated. However, substantial amplification can occur when the material is placed in the vicinity or in contact with a backing plate.[1,2] If porous materials are used as barriers to protect structures, measurement of the total stress transmitted to the backing wall is more important than the pressure in the fluid phase. Such measurements have been reported in cases of polymeric (flexible) foams and granular materials under shock compaction.[11,15]

In a series of experiments Yasuhara *et al.*[16] investigated the effect of porosity and the internal structure on the total stress at the back wall. For all foams tested in these experiments the maximum transient total stress at the back wall is larger than the pressure behind the reflected shock off a rigid wall, which is usually designated in the x-t diagram as P_5. The final converged value of the total stress reaches P_5. It was also observed that there is a delay time for the total stress rise compared to the rise of the pressure upon the reflection of the incident shock wave off a rigid wall suggesting that the stress wave transmitting through the foam decelerates as it moves within the foam.

Extensive work has also been conducted in shock-granular material interaction. Unlike flexible foams, the granular materials have much smaller porosities and the compression that they experience upon the impact of a weak shock wave is negligible. It appears that the boundary interaction affects the total stress profile only for a short distance from the edge of the sample, i.e., only a few granular samples.[17] Ben-Dor *et al.*[18] conducted a series of experiments on different types of granular materials where pressures in front, behind, and within the granular material were recorded during the impact with weak shock waves. The stress within the granular materials and the total stress at the back wall were measured. It was observed that the pressure behind the shock wave reflected off the material front face reaches the value of P_5. Similar to the flexible foams, two separate waves propagate within the material skeleton and the pore gas between the granules of the sample. Based on the recorded signals of pressure and stress, wave diagrams were reconstructed revealing the presence of a transmitted wave, a compaction wave and a rarefaction wave. For materials with a larger permeability the transmitted wave travels

at a constant velocity which is governed by gas filtration. For low permeability materials, the transmitted wave path strongly depends on the compaction wave propagation. Unsteady stress profiles similar to those in flexible foam experiments were observed at the back wall followed by vibrations. The amplitude of the peak was higher in materials having a low effective density, and a small permeability coefficient. Slowly rising precursors were also observed in the stress signals as well as the pressure signals of some of the samples, which are due to the traveling gas compression waves. The amplitude of the precursor decays along the material due to the drag between the skeleton and the moving gas. However, unlike flexible foams, it was observed that the compressive stress was well preserved in the material during the postpeak period and for most of the samples it is higher than the reflected gas pressure ahead of the layer, which reaches P_5.

In order to understand the role of the gas flow within the granular medium on the stress formation, Britan & Ben-Dor[17] conducted experiments in which the gas flow into the samples was blocked by placing a thin plastic film on the front edge of the granular sample and the total stress at the back wall was measured and compared to the case with no film in front of them sample. The signals of the effective stress at the back wall as well as the pressure history above the sample reach the value of P_5, as was the case in the previous experimental study by Ben-Dor *et al.*[18] It was concluded that the gas flow in the granular material due to the impact of the shock on the sample, is the main reason for the formation of total stress at the end-wall which increases its peak value due to the additional compressive drag force that is applied on the granular particles. Furthermore, since the gas flow in the sample is associated with energy losses, its influence on the particle–particle interaction decreases with distance along the sample and the same behavior is observed in the effective stress. The most important result was obtained by comparing the effective stress signal with the pressure that is applied on the sample's front face, which shows that the effective stress at the end wall is much smaller than the applied pressure on the sample, unlike the case of flexible foams. Thus, there is an attenuation of the shock wave which reflects at the granular layer face. The authors argue that filtration process causes energy loss in the transmitted stress wave in the granular material, thus reducing the stress value. It was concluded that for each type of granular material there is a specific length which results in the maximum peak of the total stress. For short layers, the peak stress amplitude can be restricted by the arrival of the rarefaction wave. This effect was more pronounced in samples with larger permeability. According to Ben-Dor,[18] for long layers the peak profile of the total stress is mostly governed by the elastic bulk resistance to the compression in course of the particle–particle interaction.

The present contribution is a part of a series of papers reporting on the results of a research program focusing on the physics of shock waves interacting with monolithic and composite materials,[19,20] structures,[21,22] or porous materials including nanoscale interactions.

Our research focuses on the effects rigid open-cell metallic (or ceramic) foams have in the transmission of stresses to a structure. In the few experiments that have been on rigid open cell porous materials, only gas pressure inside the porous material and at the backing wall has been conducted. As a first estimate, the transmitted stress can be predicted by using the theory of linear elastic wave propagation across a change of media. Therefore, the aim of this work is to study experimentally the contribution of the flowing gas in the pores to the stress applied on the structure due to shock wave loadings and to compare the results with the ones calculated from the equations of linear elastic wave propagation across interface between different acoustic impedance media. In the process, the degree of the deviation of the porous material from elastic solid will be examined. In the experimental data analysis, the measured time-dependent signals were decomposed into two components, one with low frequency content which is argued that it is associated with Biot's slow wave and one with high frequency contributions which corresponds to the fast wave propagation. It is also argued that this decomposition can differentiate the effects of gas pressure in the pores from the stress in the matrix of the porous medium.

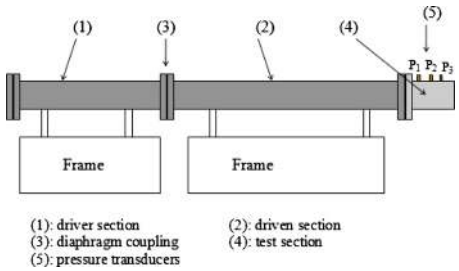

FIG. 1. (Color online) Schematic of the shock tube (not to scale).

II. EXPERIMENTAL SETUP AND TECHNIQUES

A. Shock tube

The experiments were carried out in the shock tube shown schematically in Fig. 1. It consists of a high pressure section (driver section) separated by a diaphragm from the low pressure section (driven section) and the working/test section. The shock tube's driver section is made of steel with inner diameter of 8.9 cm and length of 8.3 m. The driven section is made of stainless steel with inner diameter of 4.445 cm (1.75 in.) and a total length of 3.320 m. The test section is made of Aluminum 6061 with an inner diameter of 4.445 cm (1.75 in.) and 30.5 cm long, and is fitted with several instrumentation ports. A characteristic feature of this shock tube is that the length of the driver section can be varied. This is done by moving the piston connected to a power screw within the tube. By altering the length of the driver section, the strength and duration and thus the impulse of the waves generated in this facility can be controlled more precisely. The position of the piston in the present experiments was selected so that the arrival of the expansion waves in the test section is delayed as much as possible.

TABLE I. Properties of porous aluminum samples used in the experiments.

Nominal porosity (%)	Actual porosity (%)	Actual density (Kg/m^3)	Young's Modulus E (GPa)	Cell type	PPI (pores per inch)	Diameter (cm)	Length (cm)
90	91.6	226.8	0.50	Open	40	4.43	2.54
80	81.0	513.0	2.54	Open	40	4.43	2.54
70	72.0	756.0	5.50	Open	40	4.43	2.54
60	60.4	1069.2	11.00	Open	40	4.43	2.54

B. Sensors and instrumentation

High frequency response miniature pressure transducers fabricated by Kulite, model XCL-072, and semiconductor strain gages developed by Micron Instruments (type SS-060–033–1000PB-S1) were used in the present investigation which required high temporal and spatial resolution to detect fast moving wave patterns. The instrumentation comprises of data acquisition system for digitizing pressure and strain signals, amplifiers, filters, and power supplies for operating pressure and strain gages. All data were digitized by 4 National Instruments Analog-to Digital-Converters model NI PCI 6120 with 16 bit resolution and up to 800 kHz per channel sampling rate for a total of 16 channels. The data acquisition system was triggered by the arrival of the shock wave at the location of the most upstream wall pressure transducer. Several EG&G PARC preamplifiers/filters (Model 5113) were used for signal conditioning before the digitization of the signals.

The strain gages employed in this research are of high sensitivity (50 to 75 times greater than foil gages), small physical size with dimensions $0.84\times0.2\times0.01$ mm^3 [active length$\times$width$\times$thickness] and high frequency response. A constant current battery operated circuitry was used to excite the strain gages with a very low current of 0.6 mA through each of the strain gages. A constant current circuit was used because it is most effective when dynamic strain is being measured. In these cases a dynamic load produces a change in the resistance of the strain gage and only the time varying component of the output needs to be measured, whereas slowly varying effects such as thermally induced changes such as changes in lead resistance due to temperature variations would be eliminated. Using this configuration, temperature drifts become nearly negligible.

The frequency response of the pressure transducers was close to their resonance frequency of 150 KHz while that of the strain gages was about 20 kHz. The strain gages were calibrated *in situ* by firing the shock tube with different pressures.

C. Sample properties and bulk parameters

Aluminum alloy foams fabricated by ERG Materials and Aerospace Corporation were used in the present experiments. Tables I and II list their physical properties and bulk parameters. Porosity is defined as $\Phi=1-\rho_s/\rho$ where ρ_s/ρ is the ratio of the density of the sample ρ_s to that of zero porosity massive aluminum ρ. The values of the nominal porosity have been provided by the manufacturer while actual porosity values are those measured in the particular samples. The diameter of the foam specimens was slightly trimmed by sand paper to fit the shock tube. The correlation equations for metallic aluminum foams derived in Dukhan[23] were used to estimate the values of permeability and inertial drag coefficient shown in Table II. The inertia coefficient is associated with the nonlinear drag law known as Forchheimer term. Samples with four different porosities were tested under the load imposed by the same constant strength shock wave which is described in terms of pressure or Mach number.

The compression strength of the aluminum foam is 367 psi (2.53 MPa). The maximum load applied on the samples is 150 psi (1 MPa). Thus the foams will experience elastic loading.

D. Test setup for measurement of pressure along the porous material

Several experiments were conducted to characterize individually the behavior of the porous aluminum samples during their interaction with shock waves. In these tests the time-dependent pressure was measured by using pressure transducers. Details of the working section with the porous material specimens and the associated instrumentation used to conduct the experiment is schematically shown in Fig. 2(a). The pressure transducer P1 was used to measure the strength of the incident shock wave as well as the pressure changes due to the reflection of the shock wave off the sample. The pressure transducer P2 was used to monitor the pressure inside the pores of the sample and transducer P3 was used to measure the pressure after the sample. The shock tube in this arrangement was open to atmosphere. Each sample was placed in the shock tube such that the midsection of the sample is coincident with the center of the P2. The sample was secured in its position using copper tipped set screws [see Fig. 2(b)]. The set screws penetrate into the sample to a depth of 3.2 mm (1/8″ in.) to ensure sufficient clamping force on the sample. Two additional experiments

TABLE II. Flow and wave propagation related properties of porous aluminum samples.

Nominal porosity (%)	Permeability K (m^2)	Inertial coefficient c_d (m^{-1})	Compression wave speed (m/s)	Acoustic impedance (Kg/m^2 s)
90	1.85×10^{-8}	16	1485	3.37×10^5
80	3.40×10^{-9}	2560	2225	11.4×10^5
70	8.06×10^{-10}	4720	2700	20.4×10^5
60	1.26×10^{-10}	7500	3210	34.31×10^5

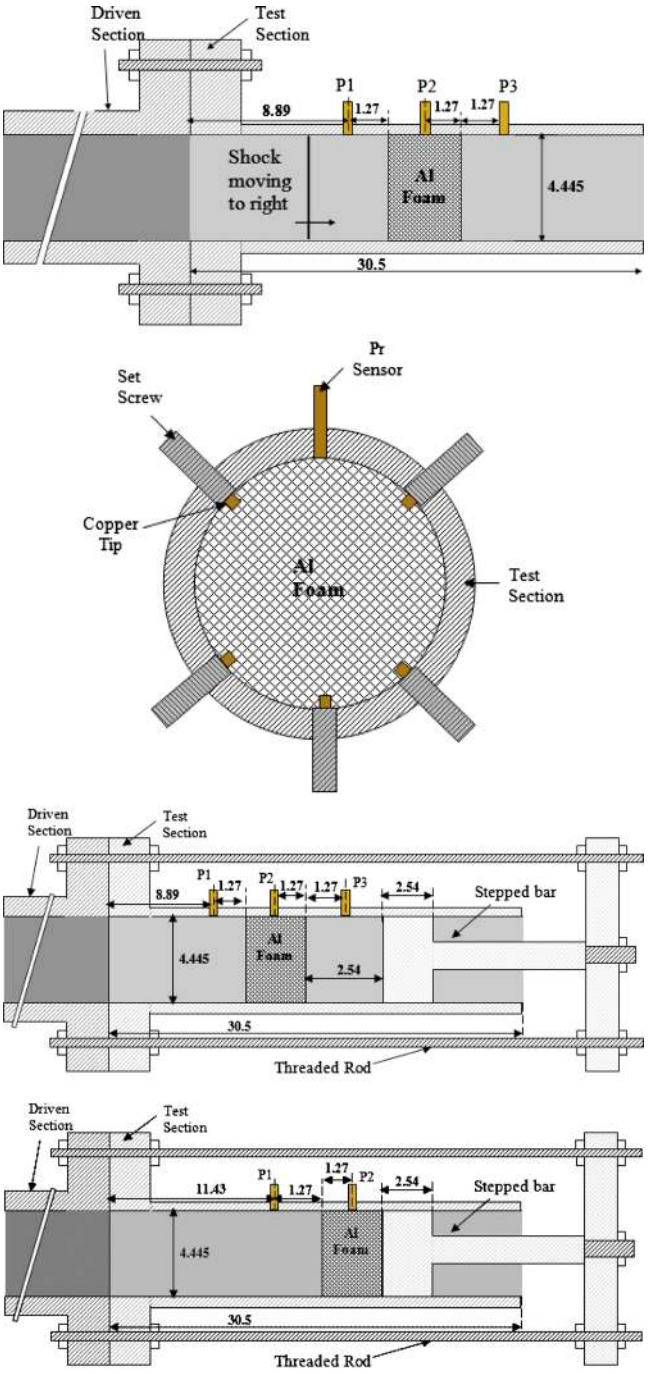

FIG. 2. (Color online) (a) Expanded view of test section with instrumentation in an experimental setup to measure pressure across porous material (all dimensions in centimeter). (b) Schematics of fixture to hold the porous Aluminum sample. (c) Closed end wall with specimen at 2.54 cm distance upstream of wall. Transducer P2 is located at the mid section of the specimen while P3 is placed midway of the gap between the sample and stepped bar. (d) Closed end wall with specimen in direct contact with the end wall. Transducer P2 is located at the mid section of the specimen.

were conducted in which the shock tube was fitted with the end wall. In the first experiment, shown schematically on Fig. 2(c), each porous material sample was placed at a distance of 2.54 cm from the end wall and in the second the material was in direct contact with it as shown in Fig. 2(d). These experiments provided data to compare qualitatively with previous investigations by Seitz & Skews[1].

E. Measuring stress transmitted to an elastic substrate

A shock-tube setup with a modified Hopkinson Bar was designed and developed for investigating the stress transmitted to an elastic substrate. This unique facility comprises of an instrumented strain bar with step load input provided by the shock tube. A schematic sketch of the test facility is shown in Fig. 3. This test facility provides a unique platform for characterizing the material response under shock wave loading.

The main part of this configuration is the 3.6576 m (12 feet) long, 4.445 cm (1.75 in.) diameter aluminum 6061 bar. The horizontal alignment of the rod is ensured by Teflon bearings which are located close to the ends of the rod. The weight of the rod is supported by two half Teflon bearings which are located in the middle. Teflon bearings where used to minimize the friction between the rod and the bearing. The rod is thus free to move in the longitudinal direction. The front face of the rod was machined to provide a perfect smooth contact between the rod and the samples. Figure 4 shows a close-up view of the test section with the Hopkinson bar at its end. The pressure transducer, P1, was used as a triggering signal to initiate data acquisition.

The influence of bending of the instrumented rod under its own weight has been compensated for by mounting four strain gages, with two of each pair placed in diametrically opposite sides. The pairs were located on the same vertical plane but at different locations along the rod (see Fig. 3). By taking the average of each pair of time-dependent strain signals, bending effects are removed from the recorded strains. An arresting mechanism comprising of sand bags was placed on the back of the rod to prevent the rod from moving out more than a desired amount. The most challenging part in setting up this arrangement was the alignment of the rod with respect to the shock tube, which was achieved by using solid state laser beams.

The shock impact on the front face of the Hopkinson bar generates an elastic stress wave which starts to propagate in the longitudinal direction and becomes one dimensional after a few diameters of traveling distance. The governing equations for one dimensional wave propagation in a Lagrangian frame are $\partial V/\partial t+1/\rho\partial\sigma/\partial x=0$ and $\partial\epsilon/\partial t+\partial V/\partial x=0$ where ε is the strain, V is the particle velocity, σ is the stress, and ρ is the density of the bar. The first equation represents the momentum balance while the second represents the mass conservation and compatibility requirements. The momentum balance shows that the net forces acting on an element are balanced by inertia. Classical wave propagation theory in elastic media[24] has shown that the particle velocity V is much smaller than the wave speed C since $V=\varepsilon C$ and that each of the terms in the equations above are extremely small throughout the field except across the wave front. The volume behind the moving stress wave is always under a constant stress determined by the jump conditions across the shock through $\sigma=\rho VC$ with negligible particle acceleration.

The acceleration of the bar as a whole takes place on a time scale which is much larger than the time scale associated with the wave propagation. The motion of the bar does not commence before the wave bounces back and forth sev-

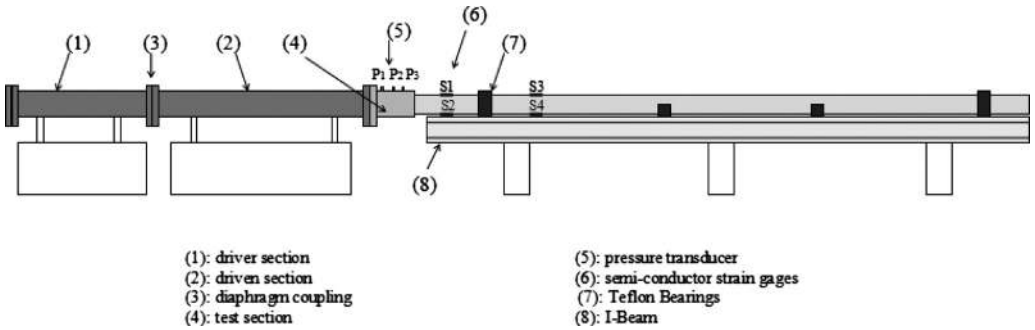

FIG. 3. Schematic of the experimental setup for stress transmission measurements.

eral times. The time-scale of the wave phenomena under investigation is of the order of 100 μs or less which is much smaller than the time scale of the motion of the Hopkinson bar. The particle velocity estimated to be 0.064 m/s and the corresponding displacement of the bar was only 6.4 μm.

Additional tests were carried out to estimate the amount of friction which could be exerted by the bearings on the bar. Strain gages ahead and behind the bearing show no variation of ε with x. The recorded time-dependent signals of ε from these two positions 0.36 m apart overlap with each other. Had friction or inertia effects been present, the stress gradient would not have been zero, i.e., $\partial\sigma/\partial x \neq 0$. Under these circumstances acceleration has no role on the phenomena under investigation. Eventually the bar moves 1 or 2 cm and its motion is arrested by the sand bag. However, there is no force from the sand bag in the initial stages of the wave propagation even in the case the bag is physically in contact with the bar before the shock loading, before the arrival of the shock at the end of the bar. If the bar were initially set in contact with the bag, a contact reaction force would have been developed after the arrival of the elastic shock at the end of the bar. In that respect, the phenomena associated with initial stages of the wave propagation within the bar are really independent of whether it is in direct contact or not with the sand bag.

In order to prevent any shearing effect between the wall of the working station and the surface of the rod, the working station's inner diameter was increased by 0.1270 mm (0.005 in.). Furthermore, in order to ensure that the sample is not in contact with the wall of the tube, the outside diameter of the samples were reduced by approximately 2 mm using a sand belt. Additionally, in order to prevent leaking of fluid flow through the gap between the test section's internal surface and the cylindrical side of the samples, the sides of the samples were coated with a two component epoxy as Fig. 5 shows.

Particular emphasis was given to the question of how the additional viscoelastic material used to glue the samples on the Hopkinson bar could affect the stress transmission to the bar. Several arrangements were tested. In the first arrangement the whole frontal surface of the bar was covered with glue uniformly and then a 0% porosity sample was carefully placed against. No difference in the transmitted stress signals were observed between this arrangement and the case of no sample in front. In that respect, it appears that the glue has no effect in the stress transmission. However, it is not certain that this will be true in the cases of low density, i.e., high porosity samples with low acoustic impedance. In order to address this issue a second arrangement was investigated in which all contacts of the solid phase of a 90% porosity sample were glued on the bar. Since reasonable results were obtained in this arrangement, it can be concluded that the effect of glue on the stress transmittal is minimal in the range of sample impedance used in the present investigation.

Two sets of experiments were conducted by attaching the porous aluminum sample to the instrumented rod. While in the first set, the front face of the aluminum foam was kept open [as shown in Fig. 5], in the second, the front face of the samples were covered with a thin layer of aluminum tape as shown in Fig. 5. This experiment was carried out in order to understand the role that the gas flow through the pores has on the total stress transmitted to the rod. In addition, an experi-

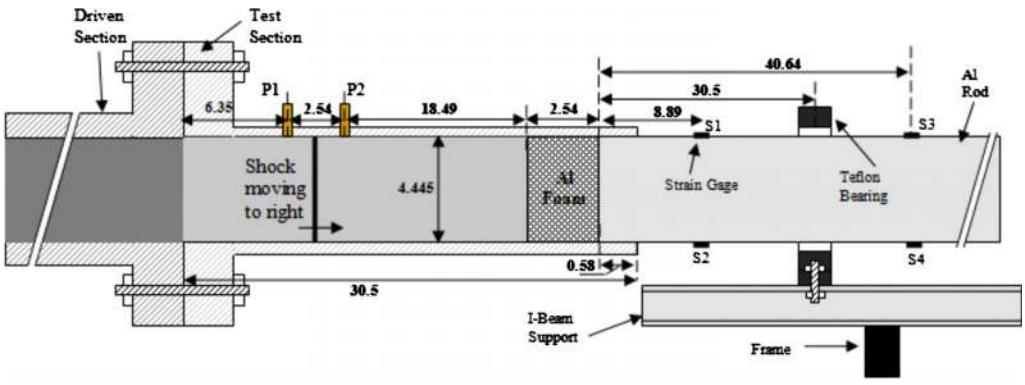

FIG. 4. (Color online) Close up view of the porous material-rod interface.

FIG. 5. (Color online) (a) Aluminum foam sample (left), (b) Sample's side coated with epoxy (center), and (c) Sample's face covered with aluminum tape (right).

ment with an aluminum 6160 nonporous sample ($\Phi=0$) was conducted in order to confirm the validity of the experimental setup. This sample was machined to the size of the porous samples and it was placed in front of the rod.

F. Strain gage calibration

The strain gages were calibrated in a series of experiments in which their voltage output V_s was mapped on a known stress/strain field. Shock waves of known strength impacted the Hopkinson bar in the absence of porous specimens and the voltage across the gages was recorded. Since all deformations in the present experiments were elastic, stress values σ were converted to strain ε through Hook's law. Typical calibration curve is shown in Fig. 6 where the voltage measured after the passage of the stress wave has been plotted against the known strain. A linear relation between voltage and strain was derived through a best fit of the experimental data and used later in the data reduction.

Additional verification of the calibration was provided by recording the reference voltage V_{s0} across the strain gage before each experiment which provided the reference level of the initial gage resistance/length ΔL_0. The output voltage of the strain gage measured during the experiment is $V_s=R_0I+\Delta RI=V_{s0}+\Delta V_s$ where I is the constant current through the loop. Since $\Delta V_s/V_{s0}=\Delta R/R_0=G_F\Delta L/\Delta L_0=G_F\varepsilon$ where G_F is the known gage factor (=155) provided by the manufacturer, the local strain ε can be estimated through the relation $\varepsilon=(\Delta V_s/V_{s0})/G_F$. This technique is free of any possible inertia effects in the rod and provided the means of a second type of calibration which differed only 14% in slope from the first one that involved a direct mapping of voltage to known stress field.

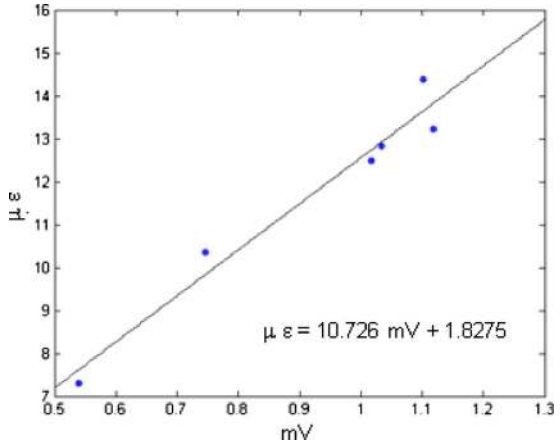

FIG. 6. (Color online) Typical strain gage calibration.

III. INDIVIDUAL SAMPLE CHARACTERISTICS UNDER SHOCK LOADING

Figure 7(a) shows the pressure signals obtained during individual tests of the porous samples in the open end setup of the shock tube as shown in Fig. 2(a). The Mach number of the incident shock wave in these experiments was $M_i=1.4$. As the incident shock wave impacts the front surface of the porous material, a partially reflected shock wave is formed propagating in the upstream direction and a transmitted shock/compressive wave propagating inside the porous sample. The signals recorded by P1 placed in front of the foam show a two-step pressure increase; the first one is associated with the passage of the incident shack wave while the second is associated with the passage of the shock wave that is reflected off the front face of the porous material. In the case of reflection of the shock wave off a rigid wall, the pressure region following the sharp rise due to the reflected shock is constant. However, in the present case, the pressure rise exhibits a slow rise feature in the asymptotic transition from the sharp increase to the constant pressure level. This gradual build up of pressure is due to an extended reflection process of the significantly slowed down by friction incident shock inside the material which generates compressive waves traveling upstream that emerge from the front interface and further increase the pressure behind the reflected shock wave. This behavior has been also found in Refs. 1 and 4.

The pressure signals recorded by the P2 transducer, which was measuring the pore pressure, have a small sharp rise in the beginning, sign of the passage of the transmitted wave, followed by a gradual pressure build up to an asymptotic value which is lower than the reflected pressure off the front face of the sample. Transducer P3 measured the pressure at a distance of 1.27 cm behind the sample. It can be seen that the incident shock wave attenuates as it is transmitted through the sample and becomes a fully dispersed wave once it leaves the sample. Similar observations were made by Kitagawa *et al.*[25] in their study of shock wave through polymeric foams.

Even though the pressure traces for the 90% porosity sample have similar qualitative features relative to the 80% sample as described above, there are some obvious quantitative differences. Because of the lower porosity, lower permeability and thus higher inertial drag coefficient, the volumetric gas flow within the 80% porosity sample is smaller and more diffusive than in the 90% sample. Therefore, the pressure within the 80% sample exhibits a more gradual rise to its asymptotic value; the amplitude of the sharp pressure rise at the leading edge of the P2 signal is much smaller than the 90% one and diffuses faster. As a result, a lower amplitude fully dispersed wave leaves the 80% sample in contrast to the 90% sample where a pressure wave exits the sample with higher amplitude and a detectable sharp front.

Also evident in Fig. 7(a) is the difference in the strength of the reflected shock waves between the two cases with

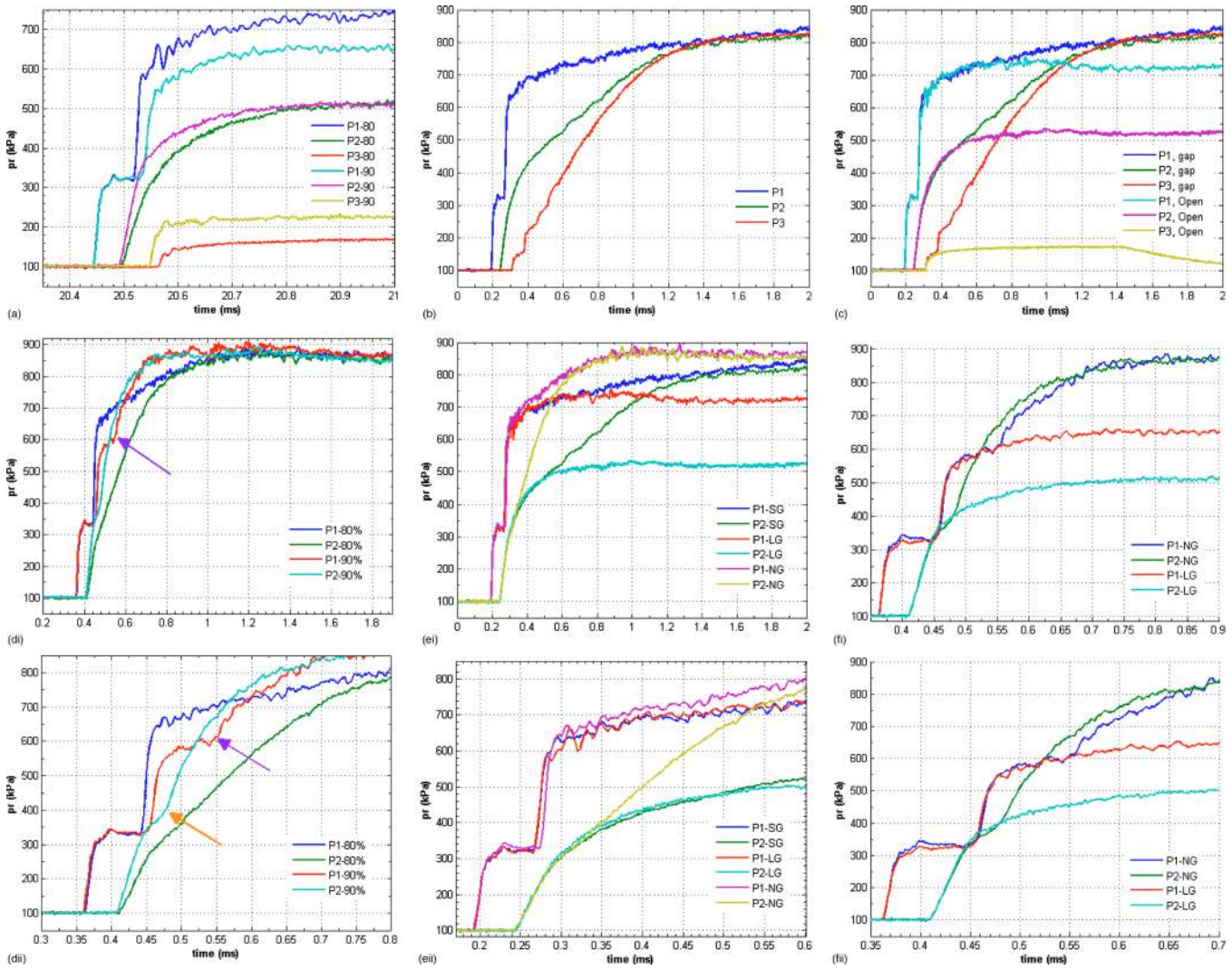

FIG. 7. (Color online) (a) Pressure histories of the gas before, inside, and after the porous aluminum foams with Φ=80% and 90%. (b) Pressure signals obtained at locations upstream, inside, and downstream of the 80% porosity sample placed at 2.54 cm from the end wall. (c) Comparison of the pressure signals obtained with porous sample at 2.54 cm from the end-wall with those obtained in experiments with open-end tube for the case of 80% porosity foam. [(d) (i)] Pressure signals histories for the 80% and 90% samples in the case of no gap between samples and end-wall. Transducer P1 is located 1.27 cm upstream of sample and transducer P2 is located in the wall above the sample 1.27 cm upstream from end wall. (ii) Expanded view of Fig. 7(d)(i). [(e) (i)] Comparison of the pressure signal for the no gap (NG), small gap (SG), and large gap (LG) experiments for the 80% porosity foam. (ii) Expanded signals shown in Fig. 7(e)(i). [(f) (i)] Comparison of the pressure histories for the no gap (NG) and large gap (LG) experiments for the 90% porosity foam. (ii) Expanded signals shown in Fig. 7(f)(i).

different porosity samples as this is shown in the signals recorded by transducer P1. Because of the denser structure of the 80% sample, the initial pressure jump across the reflected shock wave is higher than that of the 90% sample. The lower permeability and higher relative density (less porosity) of the 80% sample, results in more wave interactions inside the sample than in the case of the 90% porosity sample. As a result stronger compression waves are generated in the 80% sample that emerge from the frontal surface of the foam and coalesce with the reflected wave thus increasing its strength. In addition, since the shock/compression wave traveling downstream is damped faster and its speed reduced more, that will also contribute to the increase in pressure.

The attenuation of the shock wave after its passage through a porous medium can be expressed by K_a defined as the ratio of the pressure behind the transmitted wave, P_t to the pressure behind the incident shock wave, P_i: $K_a = P_t/P_i$. Table III list the values of K_a for the two porous aluminum foams tested. As is expected, the value of Ka for the 80% sample is lower since its permeability is lower, thus the energy loss is higher than in the case of the 90% porosity sample.

A second set of experiments was carried out with the same incident shock strength $M_i=1.4$ in which the sample was placed at distance of 2.54 cm upstream of the closed end wall of the shock tube. Figure 7(b) shows the pressure sig-

TABLE III. Values of $K_a=P_t/P_i$ for 80% and 90% samples.

Nominal porosity (%)	K_a
80	0.53
90	0.71

nals of the flow as recorded by the pressure transducers P1 through P3 in the case of the $\Phi=80\%$ porosity sample. These signals exhibit the same qualitative characteristics with those obtained in the case of open end wall. However, a unique difference is that all pressure signals in the experiments with the small gap between the sample and the end wall converge to the same asymptotic value after some time which is the p5 value of 840 kPa behind the reflected shock off the end wall in the absence of specimens in the test section. This is probably expected, since the flow is confined and thus the pressure continues to build up due to successive reflections off the tube end wall and off the end surface of the porous material until there is no pressure difference across the porous sample. Evidence of this interaction can be found in the details of the P3 signal which monitors the flow inside the gap. As can be seen it contains several incremental pressure rises. The first pressure rise is due to the passage of the compression wave that leaves the porous material. As mentioned earlier, the wave is fully dispersed, since it does not contain any sharp jump. The second pressure rise is due to the reflected wave off the rigid end wall and seems to be sharper than the initial rise since it is reflected off a rigid surface. The pressure wave travels back and forth inside the gap (as seen from the numerous pressure rises) and becomes weaker as it travels. This can be seen from the decrease in level of the pressure increments, while at the same time due to the pressure gradient across the sample, there is continuous but gradual pressure feed into the gap until there is no more pressure difference at which point the gas becomes stagnant.

Additional quantitative differences can be depicted in Fig. 7(c) where the signals obtained in the case with a small gap between the end wall and the sample are closely compared with those obtained in the case of open end wall. For the present discussion, the experiments in the case of open end shock tube can be considered as being equivalent to having an infinitely large gap between the sample and a rigid end wall. It is very interesting to observe the degree of initial overlapping of the corresponding signals between the two cases. This overlapping is most pronounced in the P1 signals and least pronounced in the P3 signals where most of the quantitative difference is evident.

A third set of experiments was carried out in which the porous specimen was placed next to and in direct contact with the wall. The incident shock wave had the same strength $M_i=1.4$ as in the previous two experiments with small and large gaps.

Figure 7(d)(i) shows the pressure signals of the flow as recorded by the pressure transducers P1 and P2 for the $\Phi=80\%$ and 90% porous aluminums. Transducer P2 measures the pore pressure at the wall and it is placed 1.27 cm from the end wall. The P1 signal for the 90% porosity specimen has three distinct pressure rises with various rates of pressure increase which indicate the passage of a shock or compression waves. Usually the pressure signals upstream of the sample are characterized by two sharp pressure rises. In the experiments with zero gap between the sample and the wall, an additional pressure rise, marked by the purple arrow in Fig. 7(d)(i), is present even though it is not as sharp as the second one. If the signals are expanded in time, this feature is also evident in the P2 signal as shown in Fig. 7(d)(ii), marked by the orange arrow, albeit this third pressure jump is rather weak.

These two characteristics seem to be absent in the 80% sample. However, the presence of these two features can be verified by comparing them to the results obtained in the two previous experiments with small and large gaps. Figures 7(e) and 7(f) depict the signals of the 80% and 90% porous samples for this experiment along with the previous experimental results, respectively.

Figures 7(e)(i) and 7(e)(ii) show a comparison of the pore fluid pressure signals, obtained by P2, in the three experiments with different gap values. A smooth pressure increase can be observed in these signals up to 0.35 ms, for the three cases. After this time the pressure in the no gap case increases while there is a substantial change in its slope, suggesting a pressure rise similar to the 90% porosity data. This damped pressure jump can also be identified in the P1 signal near the 0.5 ms mark, where an added pressure effect can be observed, which raises the pressure behind the reflected shock wave slightly above the p5 value, the pressure behind the shock wave reflected off a rigid wall. Similar behavior can be observed in the signals of the 90% porosity sample for the no gap and large gap experiments, shown in Figs. 7(f)(i) and 7(f)(ii), even though the pressure jumps have sharper fronts.

What is different in the experiment with no gap, compared to the others, is that once the transmitted wave reaches the end of the sample, it impacts the rigid end wall while being inside the sample, thus reflecting a weak shock or compression wave. This reflected compression wave propagates back into the sample, i.e., in the upstream direction, raising the gas pressure behind it as the P2 signal shows, until it reaches the front face of the sample. This interaction due to the impedance step change generates a compression wave which emerges from the front of the sample into the gaseous phase. This compression wave catches up with the flow behind the initial reflected shock wave off the frontal face of the sample and increases the pressure behind it further. At the same time the interaction of the compressive reflection originated at the end wall with the front interface between the gas and the sample is expected to generate a rarefaction wave which propagates downstream, i.e., toward the end wall. This is depicted in the pressure traces as a drop in the pressure within the foam. A small and gradual pressure drop can be observed in the pressure signals of P2 in the case of the 90% porosity sample as shown in Fig. 7(d)(i). The peak of the signal occurs at about 1.0 ms time and drops by 30 kPa at 1.5 ms. This pressure drop is associated with the passage of expansion waves.[26,27] This pressure drop is rather weak in the case of the 80% porosity sample and it is rather difficult to be depicted. In general, due to the structure and physical characteristics of the 80% porosity sample (higher relative density and lower permeability) the pressure rise within the sample due to the reflected compression wave or the pressure drop due to the passage of the expansion waves is more damped compared to those in the case of 90% porosity sample.

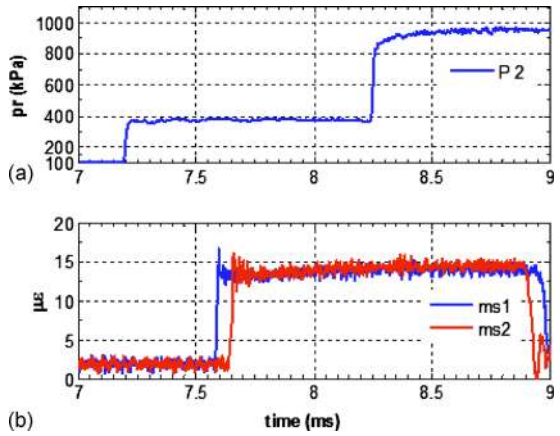

FIG. 8. (Color online) (a) Pressure (top) and (b) strain histories (bottom) for a shock wave impacting the Hopkinson bar with no samples in the tube.

IV. TOTAL STRESS TRANSMITTED TO AN ELASTIC SUBSTRATE

In this section we present the measured data of the total stress transmitted to the structure behind the porous samples due to shock wave collision. Upon the impact of the incident wave onto the front interface of the porous aluminum, a shock wave is partially reflected propagating in the upstream direction and simultaneously causing a step-wise loading on the porous sample. A stress wave is generated within the solid skeleton of the specimen while at the same time a decelerating compression wave, which initially was transmitted as a shock wave, travels through the gas fillings of the pores of the structure. The stress that is felt at the end wall-which is what the strain gages measure- is the total stress which is the sum of the internal stresses within the foam as well as the pore fluid pressure applied at the end wall.

Measurement of the stress transmitted to an elastic substrate was performed using the setup shown in Figs. 3 and 4. In conducting this set of experiments, the porous Aluminum sample was glued onto the front face of the rod. The rod was pushed inside the shock tube to a distance equal to 5.84 mm (with respect to front surface of the rod) and impacted with the incoming shock wave.

A test was conducted first in which the rod was impacted directly with shock waves in the absence of porous material specimens in front. Figures 8(a) and 8(b) show the results obtained in one of these experiments. Pressure transducer P2 is located at a distance of 18.49 cm upstream of the frontal face of the sample. Note that positive value of strain means that the rod is under compression. In the strain signals ms1 refers to the mean of the strain gages S1 and S2 and ms2 refers to the mean of the strain gages S3 and S4 where the positions of S1 through S4 are shown in Fig. 3. The longitudinal distance between the locations of the two pairs of the strain gage was $\Delta x_{sg}=31.75$ cm.

Once the incident shock wave is reflected off the front surface of the rod, a step-wise loading is applied to the rod; this in turn generates a stress wave (within the elastic region) that travels in the rod. Following the passage of the stress wave, the rod experiences a constant strain period which is associated with the p_5, the pressure behind the reflected shock wave. This compressive stress wave reflects at the end of the rod and returns as an expansive wave propagating upstream.

The oscillations following the sharp rise in the strain signal are most probably due to the dispersion of the wave in the rod. In addition the rate at which ms1 rises is slightly higher than ms2. An expanded view of the signals, not shown here, indicates a slower rate of rise of ms2 which is also due to dispersion of the wave as it travels within the rod. Besides dispersion, the Teflon bearing may also interfere with the traveling wave which might explain the small change in the slope of the initial rise of the ms2 signal since the ms2 set of strain gages is located downstream of the Teflon bearing. However, after analyzing the data with the porous samples, it was found that the transmitted wave in the rod does not become fully one dimensional at the location of the strain gages ms1 near the front face, since the strain values at the second location were found to be slightly higher than the ones closer to the rod's face. Thus, the second set of stain gages was used in the data interpretation. Nevertheless, the data in Fig. 8(b) indicate a wave propagation speed inside the aluminum bar of about 4600 m/s which is close to the value suggested in literature.

It should be noted here that in the discussions that follow the term p_5 will be encountered, i.e., the pressure behind the shock wave reflected off the front face of the rod which is similar to the case of the empty shock tube with closed end wall and no sample inserted. We define the quantity $\delta = \sigma_{t,max}/p_5$ as the amplification factor (also known as Dynamic Load Factor-DLF) that will be used in the interpretation of the reduced data. The strength of the incident shock wave was approximately 380 kPa and the incident Mach number varied between, $1.6<M<1.7$.

An additional test was conducted in which a short solid aluminum piece with dimensions identical to those of the porous samples was placed in front of the Hopkinson bar rod. This case is designated as experiment with $\Phi=0\%$ porosity porous sample. Figures 9(a)–9(c) show the results of such an experiment which can help evaluate the transmission of total stress waves through interfaces between similar materials.

The pressure traces for the two cases as expected are the same, since in both the incident shock wave reflects off a rigid wall. However, there is a time difference between arrivals of the two reflected shock waves. In the case of the empty tube the incident shock wave has to travel longer distance to the front face of the rod before reflecting, while in the case of the aluminum sample, the incident shock wave impacts the front face of the sample, and thus the reflected shock wave arrives earlier. The stress histories for the two cases are also the same even though in the case of $\Phi=0\%$, there is an interface between the rod and the sample. The reason for this similarity is due to the fact that the solid aluminum sample is of the same material as the rod and thus has the same acoustic impedance as the rod. Therefore, based on the principles of elastic wave propagation, the stress wave in the sample is transmitted to the rod with the same magnitude and no reflections are generated. Thus, it is as if the rod

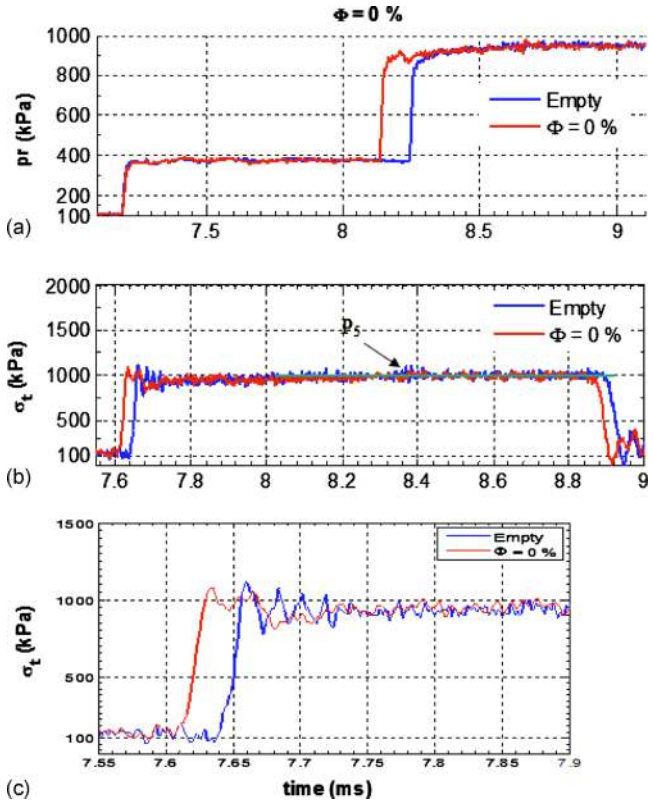

FIG. 9. (Color online) Comparison of (a) the pressure and (b) stress histories within the rod for the case of empty tube and Φ=0% aluminum sample. (c) An expanded view in time of the stress histories.

is 2.54 cm longer, a difference that explains the earlier arrival of the stress wave compared to that in the case of empty tube.

Although the whole structure behaves like a longer bar, the experimental results suggest that the interface which is practically a discontinuity in the material with imperfections in its contacts, transfers the stress waves without losses in their strength. It is also interesting to observe that the rate of rise of the stress signals in Fig. 9(c) followed the shock impact is the same in both cases suggesting that the strain gages have the same characteristic response. In addition, the readings of both strain gages, each with different calibration, converge to the value of the applied load P_5 after some time. These provide confidence that the current instrumentation and measuring techniques will be able to record and differentiate the response of different materials to shock loading.

Figures 10–13 present the results obtained in the experiments conducted with the 90%, 80%, 70%, and 60% aluminum foams. In addition, as was explained earlier in order to understand the effect that the gas flow through the pores has on the total stress transmitted to the rod, a series of experiments was carried out in which the front face of the samples was covered with a thin layer of aluminum tape. The results of these experiments are also presented in these figures labeled as "Close" in the graphs while the signals labeled as "Open" correspond to the experiments with no tape in the frontal area of the specimens where gas is allowed to flow into the samples.

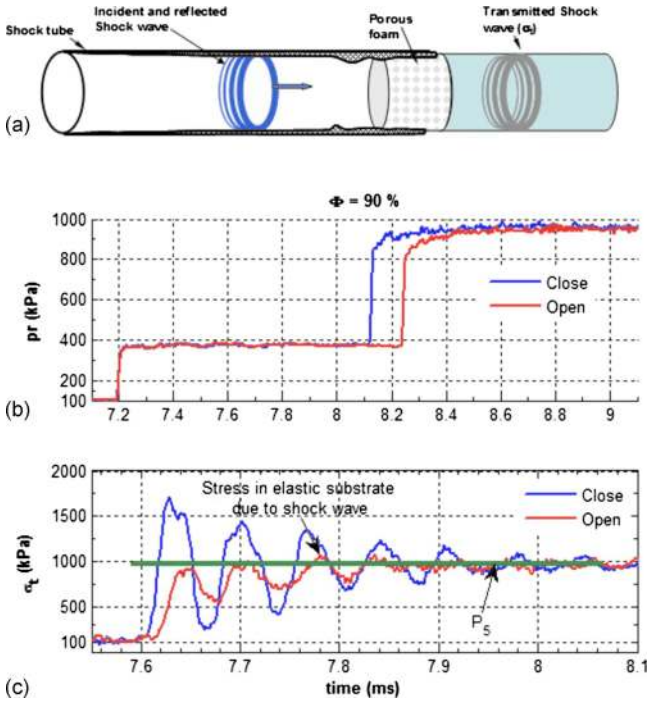

FIG. 10. (Color online) (a) Schematic of stress transmittal. Comparison of (b) pressure and (c) stress histories for the covered (close) and uncovered (open) porous sample with Φ=90%.

A. The high porosity case

Figures 10(a) and 10(b) show the results when the sample with Φ=90% porosity is placed in front of the rod. From the pressure traces shown in this figure, it can be observed that for both the Open and Close cases, the reflected pressure reaches a final value, p_5, which is comparable in magnitude to the reflected pressure obtained from the empty tube [shown in Fig. 9(a)]. The reflected shock wave off the frontal surface of the sample has a higher velocity in the case of the covered sample as it passes earlier through the P2 position. The higher strength and higher propagation velocity of the reflected shock wave can be explained by the fact that the sample behaves almost like a rigid wall upon the impact of the incident shock wave and most of the incident wave's energy is reflected. In the case of an uncovered sample, how-

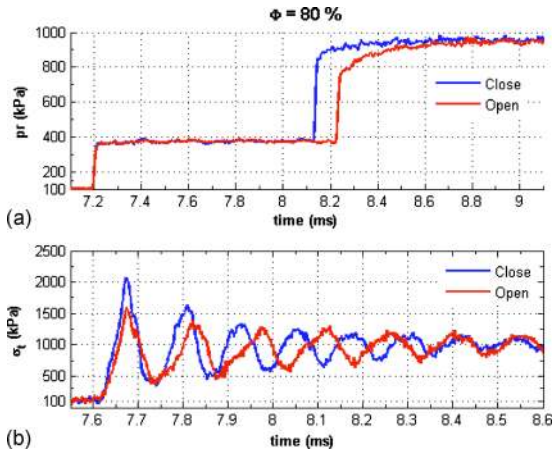

FIG. 11. (Color online) Comparison of (a) pressure and (b) stress histories for the covered (close) and uncovered (open) porous sample with Φ=80%.

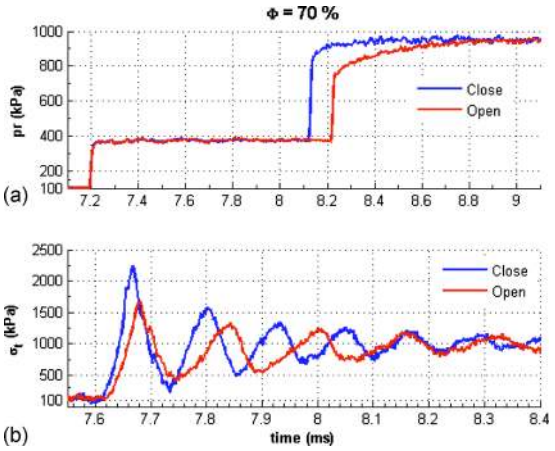

FIG. 12. (Color online) Comparison of (a) pressure and (b) stress histories for the covered (close) and uncovered (open) porous sample with Φ=70%.

ever, the shock wave reflects off a porous surface where part of the incident wave's energy is reflected and part of it is transmitted as fast and slow compression waves.[28]

The stress signals recorded from the strain gages mounted on the rod are much different from those observed in the case of the empty tube. They contain damping oscillations where the frequency of the oscillations decreases as the total stress approaches p_5, a characteristic also found in the computations of Gubaidullin *et al.*[11] The observed oscillations can be explained by considering the wave propagation within the foam. Upon impact of the incident shock wave, a transmitted (compression) wave propagates within the solid matrix of the foam and reflects once it reaches the sample-rod interface. The total stress at the rod surface then increases significantly upon this reflection, as also found in Ref. 11. The reflected compression wave travels within the solid matrix foam until it collides with the front face of the sample where a step change in acoustic impedance is present, upon which a compression wave is sent to the gas in front of the sample and a rarefaction wave travels back into the sample relieving the total stress. This process is repeated until the stress eventually reaches the value determined by p_5.

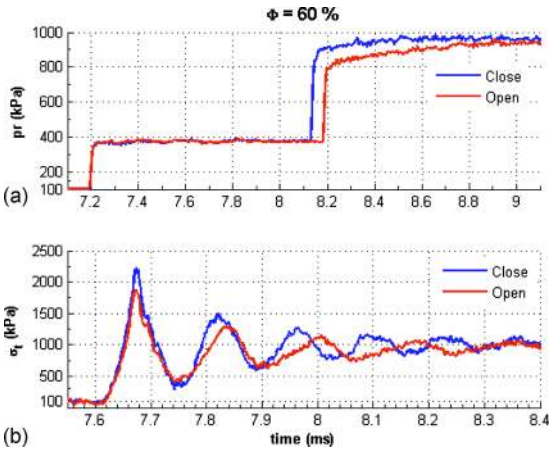

FIG. 13. (Color online) Comparison of (a) pressure and (b) stress histories for the covered (close) and uncovered (open) porous sample with Φ=60%

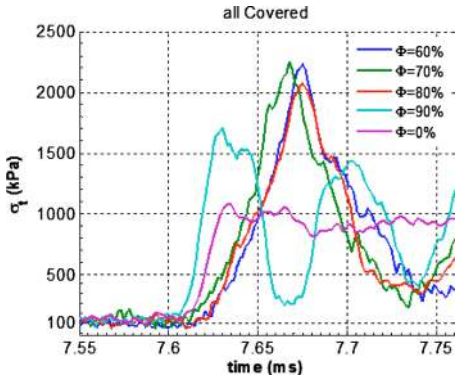

FIG. 14. (Color online) Comparison of stress histories of covered aluminum foams of various porosities.

There is, however, a significant difference between the stresses produced in the open and closed cases. In the case of a closed frontal area, the transmitted stress exceeds the p_5 value within the first cycle of the alternating load while σ_t in the open case remains below the p_5 threshold. This can be explained by considering Biot's theory of wave propagation in a poroelastic medium. In the closed case the stress wave is primarily transmitted to the solid skeleton part of the foam. Further propagation of this wave occurs by the in-phase movement of the gas in the pores and the solid skeleton. The contribution of the gas phase in the pores to the total energy carried by the foam is insignificant in this case. The gas in the pores plays a more significant role in the open case. The aluminum foam specimen used in this study has low relative density, high permeability and low inertial coefficient resulting in a high volumetric gas flow rate within the foam. Therefore, for the open case, significant amount of the gas penetrates into the foam upon impact of the incident shock wave and a stronger transmitted wave propagates within the pores. The stress wave propagation degenerates to a diffusive type in this case. The pore gas pressure influences the profile of these oscillations by introducing significant dissipation and dispersion into the propagating wave which is evident in the slower rate of stress development in the Open case.

B. The low porosity cases

Figures 11(a) and 11(b) show the pressure and stress traces in the case of the Φ=80% porosity sample. The major difference from the uncovered 90% porosity case is that the total stress signal overshoots the p_5 value right away with the onset of the load in open frontal surface case. Similar is the behavior in the cases with the 70% and 60% porosity samples shown in Figs. 12 and 13.

A comparison of the total stress signals obtained in the experiments with various porosities samples which have their frontal surface covered during the onset of the load is shown in Fig. 14. These experiments demonstrate the complexity of the stress transmission through the solid matrix of the samples since transmission of stress through the fluid phase is blocked. One observation can be made in reference to the rate of the onset of the initial load on the rod by considering the time derivative of the signals. It seems to be higher in the case of the 90% porosity sample and slowly be

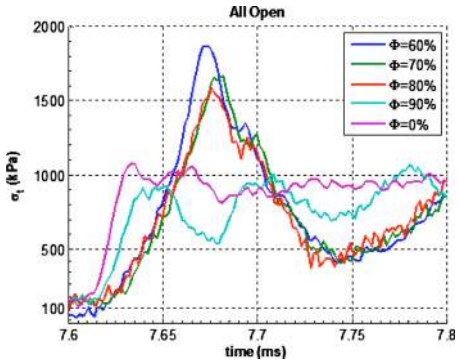

FIG. 15. (Color online) Comparison of the stress histories of uncovered aluminum foams of various porosities.

reduced with decreasing porosity. Interestingly enough in the case of 0% porosity the slope increases and the oscillatory character of the signal diminishes. A similar observation can made regarding the peak stresses in the signals. In all porous samples the peak stresses are higher than p_5. Values of the peak stress increase with decrease porosity, i.e., increased acoustic impedance, in a rather non linear way. In the present case there are two interfaces with step change in impedance. In addition to the porous specimen-rod interface there is the interface at the cover which complicates the interpretation of the data. If only the first interface were to be considered, linear theory predicts the opposite trend from that of the experimental data. It predicts that the transmitted stress increases with increased porosity, i.e., with decrease impedance. In order to correctly replicate the trend in the experimental results, the second interface in the front of the covered sample should be considered.

In Fig. 15, the total stress histories of the total stress behind the uncovered 60%, 70%, 80%, and 90% porosity samples as well as the case with $\Phi=0\%$ are compared. The rate of the total stress rise in the 60% sample is more gradual compared to the empty tube case and a delay time in the stress wave arrival exists. Also, the total stress history of 60% sample exhibits a peak value $\sigma_{t,\max}$ which is higher than p_5. Values of the amplification factor of the 60% case for the uncovered experiment have been calculated and their average is shown in Table IV along with the results obtained from the experiments with the samples of other porosities. Similar observations regarding the total stress history were made for the 70% and 80% porosity samples with some minor differences. It should be noted that for each sample several test runs were conducted and it was found that the amplification factor changes slightly from one experiment to another. As shown in the Fig. 15 the total stress signal of the 90% porosity sample shows more pronounced differences from the other three porosities. For one thing its amplification factor is less than 1, i.e., the load is attenuated while in the other three porosities it is above one even though the acoustic impedance of the 90% is less than the impedance of the other three as shown in Table II and therefore a higher stress transmission for the 90% case is expected based on the assumption of elastics wave propagation across change in media. In addition to the difference in the peak amplitude of the total stress, in the 90% case the stress has a sharper rise, higher oscillation frequency and the delay time in the stress arrival compared to the empty tube is smaller than in the other three.

TABLE IV. Amplification factor, $\delta=\sigma_{t,\max}/p_5$, for all porosities for the case of open and closed samples along with their permeability.

Φ	$K\times10^8$ (m^2)	δ_{open}	δ_{closed}
90	1.85	0.92	1.71
80	3.4×10^{-1}	1.6	2.07
70	8.06×10^{-2}	1.66	2.25
60	1.26×10^{-2}	1.87	2.23

In reference to the experiments with uncovered samples, because of the high relative density of the 60% sample, the transmitted shock wave is degenerated rather fast to a compression disturbance and the volumetric gas flow through the pores is very low. At the same time due to the low permeability and high inertial coefficient of the foam, friction and drag forces significantly affect the flow within the foam and thus the rate of pressure increase at the back wall is very gradual. The result is that for the 60% porosity sample the gas pressure within the pores does not contribute significantly to the unsteady part of the total stress history. This can be clearly seen by comparing the stress history of the covered and uncovered 60% sample shown in Fig. 13 where the stress history of the uncovered case follows the stress history of the covered case closely, indicating a minimal affect of the pore gas pressure on the unsteady part of total stress. The same observations can be made for the 70% and 80% porosity samples by looking at Figs. 12 and 11, respectively. Thus, the reason for the lower amplification of the 90% case as mentioned in (high porosity) above is due to the interaction of the pore gas with the solid-matrix.

V. FURTHER DATA ANALYSIS DECOMPOSITION AND RECONSTRUCTION

A closer look into the time dependent signals has indicated that the measured quantities are characterized by a low frequency variation which starts at the impact of the shock and ends at some time after and a higher frequency component which could be attributed to wave motion. In that respect all time dependent signals have been decomposed into two major components, one with low frequency content and one with high frequency contributions by low-pass and high-pass filtering the signals. Thus a typical quantity Q(t), where Q is the total stress or pressure, is decomposed as

$$Q(t) = Q_{LP}(t) + Q_{HP}(t). \quad (1)$$

This decomposition can be considered as a direct outcome of the Fourier series expansion in-time of the original signal and separating the two components below and above a certain frequency. In practice however, low-pass and high-pass filtering of the original signals cause some distortion around the cut-off frequency which is the same for both filtering operations. The time scales of the low frequency part and the time scales of high frequency component were reasonably far apart from each other, and therefore no information has been compromised with the data filtering. This operation is

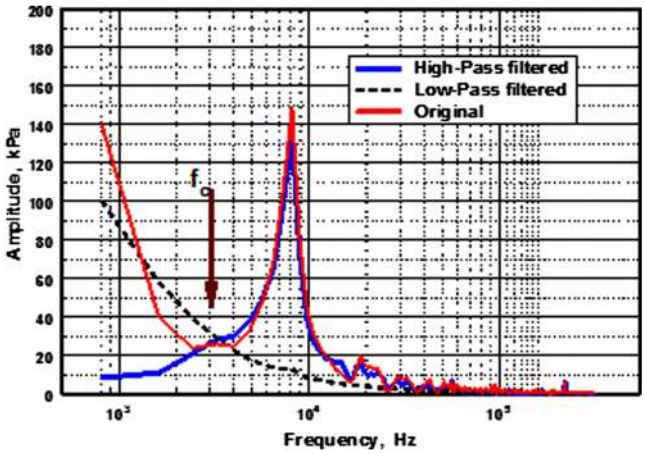

FIG. 16. (Color online) Amplitude spectra of the original, LP filtered and HP filtered stress signals in the case of porous materials with $\Phi=60\%$.

equivalent to trend removal and it is better illustrated through the amplitude spectra like the one shown in Fig. 16 which is typical of the spectra of the present stress signals. This figure shows the spectra of the original unfiltered signal, the LP filtered signal and the HP filtered. The original signal exhibits a region with extremely low amplitude between the main peak at a frequency of about 8.3 kHz and the low frequency part which is characterized by increased amplitude toward low frequencies. The cut-off frequency f_c in the filtering operations was selected to be in between these two peaks where the amplitude is small and the distortion in the nearby frequencies is not of interest. As can be seen, the decomposition depicts reasonably well the parts of the spectrum with significant amplitude.

Figure 17(a) shows the decomposition of total stress transmitted σ_t into its low- and high pass filtered components, σ_{LP} and σ_{HP}, respectively, for the case of the specimen with $\Phi=60\%$ and open frontal area. The HP filtered component does not show low frequency components or trend and it includes the high frequency components of the signal while the LP filtered component contains no fluctuations and it mainly represents the trend. In order to demonstrate the effectiveness of the decomposition, the two components have been re-combined to form the reconstructed signal $Q_{LP}(t)+Q_{HP}(t)=Q_R(t)$, which as can be seen from Fig. 17(a), does not differ from the original signal Q(t). Figures 17(b) and 17(c) show the decompositions of the stress signals in the cases of $\Phi=90\%$ and $\Phi=0\%$. All HP components of σ_t exhibit practically a zero mean value as expected. It appears that the reconstructed signal is identical to the original one indicating that the decomposition does not distort the signal. This also provides evidence suggesting the validity of this processing scheme.

Although the above decomposition is not unique, it is reasonably independent of the cut-off frequency f_c within a small range of variation. However, there is one possible physical interpretation of the present decomposition, based largely on the computational results of Gubaidullin *et al.*,[11] which is that the LP part represents the contribution from the gas pressure in the pores while the HP part is associated with the reduced stress in the matrix of the porous medium. An-

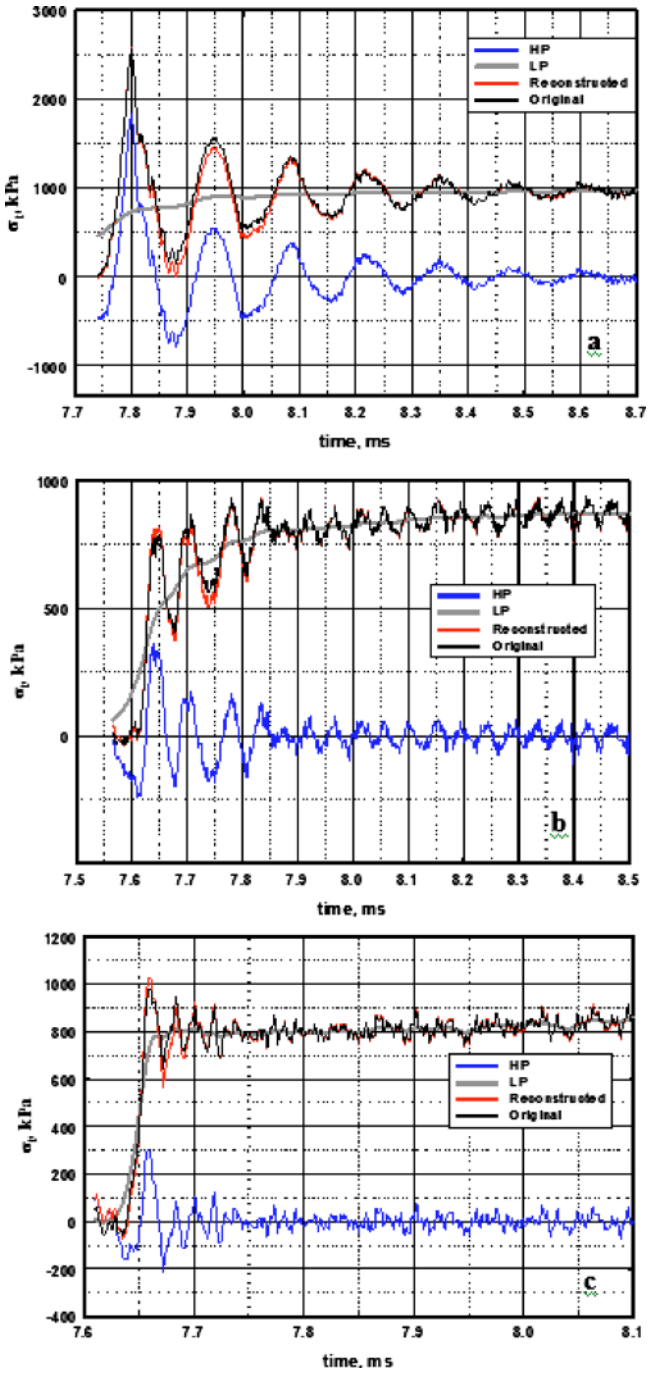

FIG. 17. (Color online) Decomposition of total stress signal into low- and high-pass filtered contributions. (a) $\Phi=60\%$; (b) $\Phi=90\%$; and (c) $\Phi=0\%$.

other possible interpretation based on the work by Brown *et al.*[28] is that the LP part is associated with Biot's slow wave propagation and the HP with the corresponding fast wave propagation.

Figures 18(a) and 18(b) show a comparison of the LP and HP contributions respectively for the three cases with $\Phi=60\%$, 90%, and 0%. The LP contributions show a different rise with time of the transmitted stress [Fig. 18(a)] which depends on the porosity of the specimen. The sharpest increase with time is observed in the case of $\Phi=0\%$, followed by the case with $\Phi=60\%$ while the case with the highest porosity exhibits the slowest rise of transmitted load with

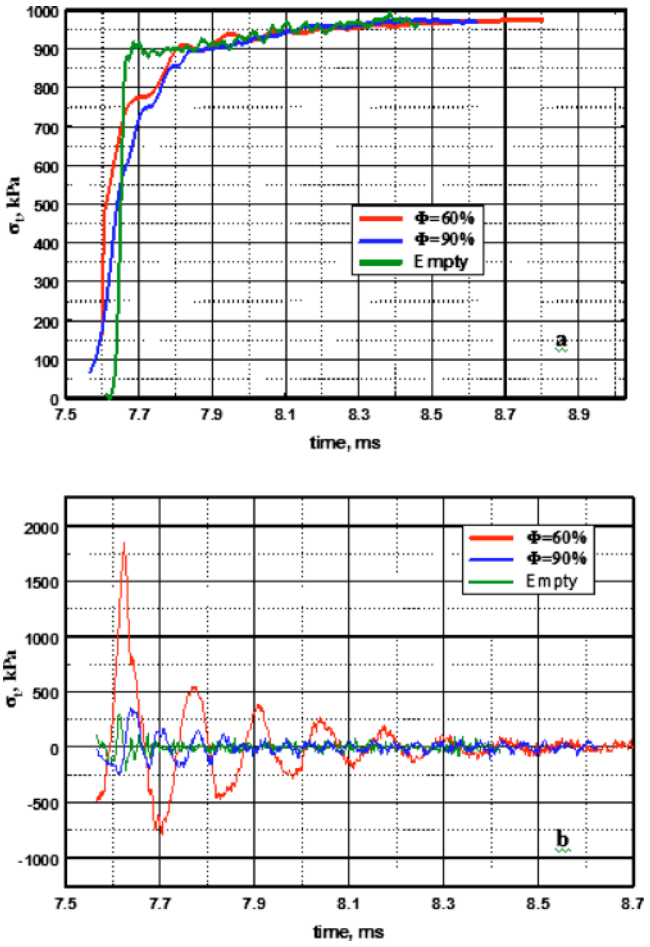

FIG. 18. (Color online) Comparison of contributing components in the cases of three different porosities. a) Low-pass filtered; b) high-pass filtered.

time. Thus the advantage of using porous materials is in prolonging the loading process of the structure and therefore in reducing its rate. The HP components shown in Fig. 18(b), however, exhibit roughly the same peak in the first cycle in the cases of Φ=90% and 0%. Thus for porous materials with high porosity, the HP component peak is not that different from the case without porous material and therefore it does not offer any particular protection to the structure. The peak load in the first cycle of the HP component of the 60% case, however, is the highest among all cases and is about five times larger than that of the 90% case.

Figure 19 shows the frequency spectra of the HP components in the three cases with different porosities. Substantial amplitude peaks can be observed in the cases of nonzero porosity. A peak at about 8 kHz can be identified in the case of Φ=60%, and two peaks at about 16 and 23 kHz in the case of Φ=90%. No particular peak can be observed in the case of Φ=0%. One major characteristic of the spectra is the significant broadening of the peak frequencies. As can be observed from the actual time dependent signals, the period increases with time in the case of Φ=60% and decreases with time in the case of 90%. The two peaks of the spectrum in the latter case indicate this frequency increase at times much later after the arrival of the impacting wave.

The data have been further analyzed to deduce the phase velocity C of the waves in the solid rod. The one dimensional

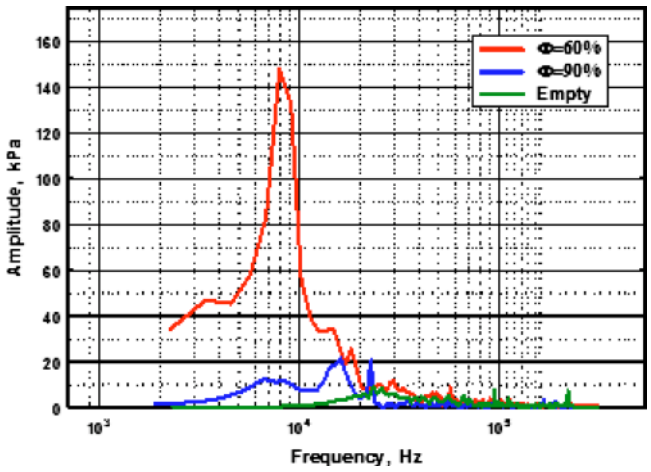

FIG. 19. (Color online) Frequency spectra of HP components in cases with Φ=60%; Φ=90%; and Φ=0%.

momentum equation mentioned previously leads to the relation $d^2u/dt^2=(E/\rho)d^2u/dx^2$ where u is the particle displacement. Solutions in the form of $e^{i(\omega t-kx)}$ lead to the dispersion equation with the phase velocity $C=\omega/k=(E/\rho)^{1/2}$ (see Kolsky[24]) where k is the wave number and ω is the angular frequency. This relation becomes $C=\lambda/T$ where λ is the wavelength and T is the period of the wave. The purpose of using this Hopkinson bar is to obtain information of the applied stress history using the measured strains from the bar. The applied stress at the front face of the bar is the result of wave interaction processes inside the porous material sample and therefore it is reasonable to look for events with $\lambda=2L$ where L is the length of the specimen since the porous sample is the controlling input of the stress load to the bar and the incident waves pass through this length. The computed phase velocity data refer to wave propagation processes inside the aluminum bar. The fluctuating stress in the bar, however, relates directly to the fluctuating applied stress since there is no stress gradient in the longitudinal direction along the aluminum bar. Thus a positive fluctuation in the stress on the bar relates to a compression event at the location of the applied stress and a negative fluctuation of the measured stress on the bar is associated with an expansion event at the interface. The generation of these large amplitude fluctuations on the measured stress at the surface of the bar is associated with the porous sample since no fluctuations were observed behind the elastic wave when the shock wave directly loads the bar in the absence of the porous sample or when the 0% porous sample was used. In that respect, the frequency and magnitude of the fluctuations measured in the stress signal on the surface of the bar are the same as those of the input pressure load at the interface. Now, the ratio λ/T has the characteristics of phase speed inside the porous sample which can be a direct outcome of the one dimensional equation mentioned above $d^2u/dt^2=(E/\rho)d^2u/dx^2$ with E and ρ now having the corresponding values of the porous samples or some other equivalent properties so that an effective phase velocity $C=(E/\rho)^{1/2}_{eff}$ can be defined.

The duration or period T of an event can be either compression, i.e., increasing σ_{HP} or expansion, i.e., decreasing σ_{HP}. Thus, two phase velocities can be identified, C_C

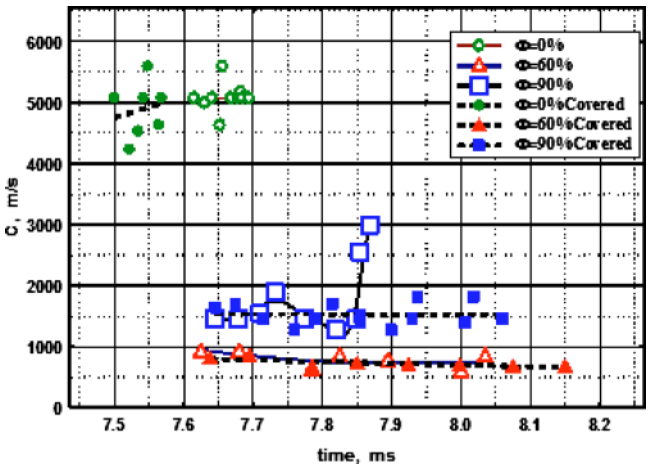

FIG. 20. (Color online) Wave propagation speeds in solid rod for various experiments with covered or uncovered porous specimens of different porosities.

$=\lambda/T_C$ during compression and $C_E=\lambda/T_E$ during expansion with $\lambda=2L$ in both cases. T_C+T_E is the duration of each loading cycle representing the period of the oscillatory stress. Figure 20 shows values of C_C or C_E obtained in various experiments in the present investigation with different specimens of different porosities with covered or uncovered their front surface. The first point of each experiment is always a compressive event and the second is always an expansive event. This sequence of alternating events is repeated in the rest of the data. In the case of $\Phi=0\%$ the average C is about 5000 m/s which is what has been documented for aluminum rods and it is close to $(E/\rho)^{1/2}$. The data show dispersion about 10% of their mean value and no difference between covered (close, 0% sample) and uncovered (open, no samples) cases. In the case of the porous specimen with $\Phi=60\%$ the data show some reduction of C with time suggesting the presence of some dispersive characteristics in the waves. There is no identifiable difference between the cases with covered and uncovered front surface. This is expected since the wave propagation speed depends on the material mainly and not on the stress transmittal surface which apparently determines the amplitude. However, a result which is not expected is that the measured values of C are considerably lower than the value of 3,211 m/s calculated theoretically from the relation $(E/\rho)^{1/2}$. One possible explanation for this behavior is the structure of the porous material, particularly its grain size and tortuosity which have not been accounted for or the presence of dispersive characteristics which invalidate the elastic wave assumption in the formula used. Probably more pertinent to the present case of a relative stiff frame is the case described in Ref. 13 where a dynamic tortuosity factor $\alpha(\omega)$ is introduced in the expression of phase velocity in the form of $C=\{E/\rho\alpha(\omega)\}^{1/2}$.

The data for the high porosity case with $\Phi=90\%$, however, reasonably agree with the theoretical value 1478 m/s obtained from the same formula. These data also show no difference in the behavior between the covered and the uncovered cases. The last two data points in the uncovered case indicate a rapid increase in the wave speed. Although this is also evident in the spectra shown before it may be due to the ambiguity associated with estimating the duration of low amplitude events. The data of wave propagation speeds in the cases with the porosities $\Phi=70\%$ and 80% are between the values of 0% and 90% shown in Fig. 20. The trend of how the experimental values of C change with Φ is the opposite of the trend predicted by the elastic wave speed formula $(E/\rho)^{1/2}$. It should be mentioned that the data presented in Fig. 20 are obtained from the HP filtered data of total strain and they agree quite well with the data estimated from the instantaneous signals of σ_t.

VI. CONCLUSIONS

The present experimental work investigated the interaction of shock waves with rigid open cell aluminum foams of different porosities and their effect in attenuating the shock wave induced stress transmitted to a structure attached at the back of the foam. The structure was represented by a 3.6 m long aluminum rod placed in the working section of a shock tube. High frequency response miniature pressure transducers and strain gages were used to measure the strength of the incoming shock and the magnitude of the transmitted stress to the rod.

Following the impact of the incident wave with the porous material sample, a shock wave is reflected while the initial disturbance in the porous material is split into the fast and slow (compression) waves. It was found that the strength of the reflected shock wave (the sharp front rise) depends on the material properties such as porosity and permeability. The asymptotic increase in pressure behind the upstream propagating wave is due to the emergence of weak compression waves from further reflections within the pores where the flow slows down. These waves catch up and coalesce with the reflected shock wave initially formed at the front face of the sample.

Because of the large compressibility ratio between air and the skeleton of the foam, the amplitude of the fast wave is very small in the gas and thus cannot be detected by pressure sensors, and it is only the slow compression wave that is measured. It was found that the propagation of the transmitted compression wave within the aluminum foam is a dispersive one where the sharp front leading edge of the transmitted wave attenuates as it travels through the aluminum foam and becomes fully dispersed as no wave structure would be present in the gradually rising pressure traces. This dispersion is a consequence of subsonic gas flow inside the aluminum foam where drag forces become the dominant factor in the solid-fluid interaction. It was observed that the lower porosity aluminum foams which have lower permeability and higher inertial drag cause more dispersion of the wave and a more gradual rise of the pressure field.

It was observed that when a gap is placed between the porous aluminum and the end wall of the shock tube, the incident shockwave attenuates as the compression wave that leaves the foam has a lower strength. Compared to high porosity and permeability foam, a fully dispersed wave leaves the low porosity and low permeability aluminum foam and the attenuation of the incident shock wave is more pronounced because of a higher energy loss in the foam.

The profile of the total stress transmitted to the rod when a porous material is placed in front differs form that of a direct shock wave impact and is characterized by damping oscillations where the frequency of the oscillations increases as the total stress approaches P_5 in the case of the 90% porosity and decreases in the cases of lower porosity samples. The transmitted stress depends on the material properties of the porous aluminum (relative density, permeability) and their length. The total stress transmitted to the rod is generally amplified and increases as the porosity decreases and the principal of elastic wave propagation across the interface between two materials of different acoustic impedance may be used to approximately explain this amplification. However it cannot explain the higher amplification factor of the lower porosity foams. This is due to the fact that this principal does not take into account the effect of pore gas flow pressure on the total stress. For a low porosity foam because of the very low and restricted volumetric gas flow rate within the foam a minimal contribution of the gas pressure within the pores to the unsteady part of the total stress history is observed; in contrast, in a high porosity foam with high permeability and low inertial coefficient, there is a high volumetric gas flow rate within the foam and thus a stronger transmitted wave propagates through the pores and a faster reflected compression wave travels upstream. This wave forms a rarefaction wave as it reaches the front of the foam and because it arrives earlier reduces the magnitude of the peak total stress.

It was found that the amplification factor depends on the material properties such as porosity and permeability. However, the relation was found to be nonlinear. Even though the porosity changes linearly, the amplification factor does not because of the nonlinear change in permeability. Moreover it is interesting to note that by using the 90% sample the transmitted stress to the rod was actually attenuated (amplification factor=0.95) even though due to the nature of a shock wave the final stress value reached was the same as the case of a direct impact of the shock on the rod.

By analyzing the total stress signals from a series of shock experiments with the front of the aluminum foams covered, it was found that the aluminum foams deviate from a linearly elastic medium and demonstrate dispersive and dissipative properties which result in damping oscillations compared to the sharp rise to a constant stress level of an elastic medium. It was also observed that beside the effect on the magnitude and duration of the initial total stress peak, the pore gas flow influences the profile of the oscillations by introducing dissipation and dispersion into the propagating wave in the solid phase due to the nonlinear nature of the solid-fluid interaction, particularly in the 90% porous foam.

Based on the experimental results of the covered foams, it was found that the highest porosity sample has the lowest amplification factor. The elastic wave propagation across two materials of different acoustic impedance may be used to explain the amplification however it cannot explain the obtained result even though this time there was no gas flow in the porous structure.

The oscillatory profile of the total stress seems to be associated with wave interactions (compression and rarefaction waves) taking place within the porous skeleton. Using the experimental data it was found that this is in fact the case for the high porosity aluminum foam while this conclusion could not be drawn for the lower porosities because the period of the oscillations are much larger than what is expected.

The stress signals have been decomposed into two components through low- and high-pass filtering, one with low frequency content which is most probably associated with Biot's slow wave propagation and one with high frequency contributions which corresponds to Biot's fast wave propagation. This decomposition has the ability to differentiate the effects of gas pressure in the pores from the stress in the matrix of the porous sample.

By using this decomposition it has been shown that wave interactions cause the oscillations in the stress in the low porosity foams. Linear theory can possibly explain the behavior of these oscillations in the 90% case but it cannot in the lower porosity cases.

ACKNOWLEDGMENTS

The financial support provided by NSF under Grant No. CC1-0800307 and ARO under Grant Nos. W911-NF-05-1-0008 and 52661-RT-ISP is greatly appreciated.

[1]M. W. Seitz and B. W. Skews, Shock Waves **15**, 177 (2006).
[2]M. W. Seitz and B. W. Skews, Proceedings of the 20th International Symposium on Shock Waves, Pasadena, California, July 1995, (World Scientific, Singapore; River Edge, NJ, 1996).
[3]B. E. Gel'fand, S. A. Gubin, S. M. Kogarko, and O. E. Popov, Sov. Phys. Appl. Maths Tech. Phys. **6**, 74 (1975).
[4]G. J. Ball, B. P. Howell1, T. G. Leighton, and M. J. Schofield, Shock Waves **10**, 265 (2000).
[5]A. Bagabir and D. Drikakis, Comput. Methods Appl. Mech. Eng. **193**, 4675 (2004).
[6]G. Mazor, G. Ben-Dor, O. Igra, and S. Sorek, Shock Waves **3**, 159 (1994).
[7]M. R. Baer and N. W. Nunziato, Int. J. Multiphase Flow **12**, 861 (1986).
[8]M. A. Biot, J. Appl. Phys. **12**, 155 (1941).
[9]A. Levy, S. Sorek, G. Ben-Dor, and J. Bear, Transp. Porous Media **21**, 241 (1995).
[10]J. Bear and Y. Bachmat, *Introduction to Modeling Transport Phenomena in Porous Media* (Klumer, Dordrecht, 1990).
[11]A. A. Gubaidullin, A. Britan, and D. N. Dudko, Shock Waves **13**, 41 (2003).
[12]J. G. M. van der Grinten, An Experimental Study Of Shock-Induced Wave Propagation In Dry Water-Saturated, And Partially Saturated Porous Media, Ph.D. thesis, Eindhoven University of Technology, 1987.
[13]D. Smeulders and M. E. H. van Dongen, *Shock Wave Science and Technology Reference Library*, edited by H. van Dongen (Springer, New York, 2007), Vol. 1.
[14]A. Levy, G. Ben-Dor, B. W. Skews, and S. Sorek, Exp. Fluids **15**, 183 (1993).
[15]M. E. H van Dongen, D. M. J Smeulders, T. Kitarnura, and K. Takayama, Proceedings 19th International Symposium on Shock Waves, Marseille, 1995, Vol. III, pp. 163–168.
[16]M. Yasuhara, S. Watanabe, K. Kitagawa, T. Yasue, and M. Mizutani, JSME Int. J., Ser. B **39**, 287 (1996).
[17]A. Britan and G. Ben-Dor, Int. J. Multiphase Flow **32**, 623 (2006).
[18]G. Ben-Dor, A. Britan, T. Elperin, O. Igra, and J. P. Jiang, Exp. Fluids **22**, 432 (1997).
[19]M. W. Gong and Y. Andreopoulos, J. Sound Vib. **313**, 171 (2008).
[20]M. W. Gong and Y. Andreopoulos, J. Comput. Phys. **228**, 4400 (2009).
[21]K. Subramaniam, W. Nian, and Y. Andreopoulos, Int. J. Impact Eng. **36**, 965 (2009).
[22]Y. Andreopoulos, S. Xanthos, and K. Subramaniam, Shock Waves **16**, 455 (2007).
[23]N. Dukhan, Exp. Fluids **41**, 665 (2006).
[24]H. Kolsky, *Stress Waves in Solids* (Dover Phoenix Editions, New York, 1953).

[25]K. Kitagawa, K. Takayama, and M. Yasuhara, Shock Waves **15**, 437 (2006).
[26]S. Xanthos, M. W. Gong, and Y. Andreopoulos, J. Fluid Mech. **584**, 301 (2007).
[27]S. Xanthos, M. W. Gong, and Y. Andreopoulos, Phys. Fluids **22**, 015111 (2010).
[28]P. J. Brown, M. Batzle, M. Peeters, S. Dey-Sakar, and G. Steensma, Shock Tube Experiments and the Observation of the Biot Slow Wave in Natural Rocks. Http://www.mines.edu/~mpeeters/shock_tube_experiments.pdf (2009).